Published in final edited form as:
Eur J Nucl Med Mol Imaging. 2009 September ; 36(9): 1510–1519. doi:10.1007/s00259-009-1158-1.

Monitor Therapeutic Response of Human Ovarian Cancer to 17-DMAG by Non-invasive PET imaging with ^{64}Cu-DOTA-Trastuzumab

Gang Niu, **Zibo Li**, **Qizhen Cao**, and **Xiaoyuan Chen**
The Molecular Imaging Program at Stanford (MIPS), Department of Radiology and Bio-X Program, Stanford University School of Medicine, Stanford, California

Abstract

Purposes—17-DMAG, a heat shock protein 90 (Hsp90) inhibitor, has been intensively investigated for cancer therapy and is undergoing clinical trials. Human epidermal growth factor receptor 2 (HER-2) is one of the client proteins of Hsp90 and its expression is decreased upon 17-DMAG treatment. In this study, we aimed to non-invasively monitor the HER-2 response to 17-DMAG treatment in xenografted mice.

Methods—The sensitivity of human ovarian cancer SKOV-3 cells to 17-DMAG *in vitro* was measured by MTT assay. HER-2 expression of SKOV-3 cells was determined by flow cytometry. Nude mice bearing SKOV-3 tumors were treated with 17-DMAG and the therapeutic efficacy was evaluated by tumor size measurement. Both treated and control mice were imaged with microPET using ^{64}Cu-DOTA-trastuzumab and ^{18}F-FDG. Biodistribution studies, immunofluorescence staining were performed to validate the microPET results.

Results—SKOV-3 cells are sensitive to 17-DMAG treatment, in a dose dependent manner, with an IC_{50} value of 68.7 nM after 72 h incubation. The tumor growth curve supported the inhibition effect of 17-DMAG on SKOV-3 tumors. Quantitative microPET imaging showed that ^{64}Cu-DOTA-trastuzumab had prominent tumor activity accumulation in untreated SKOV-3 tumors, which was significantly reduced in 17-DMAG treated tumors. There was no uptake difference detected by FDG PET. Immunofluorescence staining confirmed the significant reduction in tumor HER-2 level upon 17-DMAG treatment.

Conclusion—The early response to anti-Hsp90 therapy was successfully monitored by quantitative PET using ^{64}Cu-DOTA-trastuzumab. This approach may be valuable in monitoring the therapeutic response in HER-2-positive cancer patients under 17-DMAG treatment.

Keywords

Human epidermal growth factor receptor (HER-2); Positron emission tomography (PET); Heat shock protein 90 (Hsp90); 17-dimethylaminoethylamino-17-demethoxy-geldanamycin (17-DMAG); Trastuzumab

Introduction

The chaperone heat shock protein (Hsp90) has recently emerged as a promising target for cancer therapy [1]. The unique characteristics of HSP90 lies in the fact that it targets a

Requests for reprints: Xiaoyuan Chen, PhD, The Molecular Imaging Program at Stanford (MIPS), Department of Radiology and Bio-X Program, Stanford University School of Medicine, 1201 Welch Rd, P095, Stanford, CA 94305-5484, USA, Telephone: (650) 725-0950, Fax: (650) 736-7925, shawchen@stanford.edu.

specific set of client proteins that are mainly involved in signal transduction pathways [2]. HSP90 has been reported to play an important role in the progress of malignant disease and elevated HSP90 levels have been observed in a variety of cancers, including breast, brain, colon, and lung [3, 4]. HSP90 inhibitors, such as the benzoquinone ansamycin antibiotics geldanamycin (GA), inhibit the activity of Hsp90 and further disrupt the proper conformation of the client proteins of HSP90, including epidermal growth factor receptor 2 (HER-2), epidermal growth factor receptor (EGFR), Akt, wild-type and mutated androgen receptors (AR) [5-7].

HER-2, also known as ErbB-2 (erythroblastic leukemia viral oncogene homolog 2), is a cell membrane surface-bound receptor tyrosine kinase [8]. Overexpression of HER-2 increases cell proliferation, anchorage-independent cell growth, cell migration, and invasiveness [9-11]. HER-2 overexpression is detected in up to 30% of breast and ovarian cancers [12]. Overexpression of HER-2 has been correlated with invasive and poor prognostic features [13]. HER-2 is dependent upon Hsp90 for its stability throughout the whole life span of the receptor, including the maturation process in the ER, and during the residency of the receptor at the plasma membrane [14]. Consequently, the degradation of HER-2 upon inactivation of Hsp90 occurs from both the ER and the plasma membrane [15].

17-Allylamino-17-demthoxygeldanamycin (17-AAG) is an HSP90 inhibitor derived from GA. Both preclinical and phase I clinical studies of 17-AAG have shown that biologically relevant drug exposures can be achieved with surprisingly modest toxicity [16, 17]. However, the water solubility of 17-AAG is very poor, only around 50 μg/ml. Thus it requires the addition of organic excipients such as DMSO or polyoxyl castor oil (Cremophor) [18]. Clinical trials with 17-AAG in these excipients may confound the true maximum tolerated dose of 17-AAG and identification of the optimal dosing regimen in patients. Indeed, with low doses of 17-AAG in DMSO, there was no objective anti-tumor responses observed in several phase II trials including melanoma, hormone-refractory prostate cancer and renal cell carcinoma [19, 20]. A more water-soluble analog 17-dimethylaminoethylamino, 17-demethoxygeldanamycin (17-DMAG) has been developed and shown anti-tumor activity in human tumor xenograft models [21, 22]. 17-DMAG is currently in phase I/II clinical trials [23].

The assessment of early response to anti-cancer therapy can improve patient care by identifying patients who do not respond and therefore may not benefit from the therapy. These patients can greatly benefit by avoiding unnecessary toxic side effects and switching to different, more effective therapeutic approaches in a timely manner [24]. Since HER-2 is a key client protein of HSP90, analyzing the expression status of HER-2 will be of great help in anti-tumor therapy with HSP90 inhibitors including 17-DMAG. Traditionally, analyzing of HER-2 overexpression in surgical specimens is most commonly accomplished by either immunohistochemical (IHC) staining or fluorescence in-situ hybridization (FISH) testing [25, 26]. Despite the preselection for HER-2 overexpression based on IHC staining or FISH of a tumor biopsy, only 11-35% of patients in phase II trials responded to trastuzumab when it was given as a single agent [27]. Alternatively, various non-invasive molecular imaging modalities are under intensive investigation to provide the comprehensive diagnostic information that can improve patient management [28].

Trastuzumab is a recombinant humanized anti-HER-2 monoclonal antibody developed by inserting the CDRs of mAb 4D5 into the framework of a consensus human IgG [29, 30]. Trastuzumab has been labeled with various isotopes, chromophores, and paramagnetic nanoparticles for multimodality imaging of HER-2 expression [31, 32]. With ^{111}In labeled trastuzumab, HER-2-positive SKOV-3 tumor was clearly visualized on gamma camera scintigram imaged 72 h after injection [33]. In this study, we treated the human ovarian

cancer SKOV-3 xenograft model with 17-DMAG. After treatment, ^{64}Cu-DOTA-trastuzumab PET imaging was performed to monitor HER-2 degradation. The goal of this study was to determine whether PET imaging with ^{64}Cu-DOTA-trastuzumab, a HER-2 targeted tracer, could be used to evaluate the expression level of HER-2 and to further monitor the early response of HER-2 degradation upon anti-Hsp90 therapy by 17-DMAG.

Materials and Methods

All commercially available chemical reagents were used without further purification. 1,4,7,10-Tetraazadodecane-N, N′,N′′,N′′′-tetraacetic acid (DOTA) was purchased from Macrocyclics, Inc. (Dallas, TX) and Chelex 100 resin (50-100 mesh) was purchased from Aldrich (St. Louis, MO). Water and all buffers were passed through Chelex 100 column (1×15 cm) before use in radiolabeling procedures to ensure that the aqueous buffer is heavy metal free. PD-10 desalting columns were purchased from GE Healthcare (Piscataway, NJ). Athymic nude mice were obtained from Harlan (Indianapolis, IN) at 4-6 weeks of age. ^{64}Cu was provided by University of Wisconsin-Madison. The human ovarian cancer SKOV-3 cell line was obtained from the American Type Culture Collection (ATCC) and maintained in DMEM medium supplemented with 10% fetal bovine serum (FBS), 1% glutamine, 100 U/ml penicillin, and 100 mg/ml streptomycin (Invitrogen, Carlsbad, CA).

MTT assay

The toxicity of 17-DMAG to SKOV-3 cells was determined by MTT assay. All studies were performed with triplicate samples and repeated at least three times. Briefly, cells were harvested by trypsinization, resuspended in DMEM medium, and plated in a 96-well plate at 3,000 cells per well. At 72 h after treatment with different doses of 17-DMAG (ranging from 0.1 nM to 0.5 μM) in 0.1% dimethylsulfoxide (DMSO; Sigma, St. Louis, MO), the culture medium was replaced and 50 μl of 1.0 mg/ml sterile filtered 3-(4, 5-dimethylthiazol-2-yl)-2, 5-diphenyl tetrazolium bromide (MTT; Sigma) was added to each well. The unreacted dye was removed after 4 h and the insoluble formazan crystals were dissolved in 150 μl of DMSO. The absorbance at 570 nm (reference wavelength: 630 nm) was measured with a Tecan microplate reader (Tecan, San Jose, CA).

Flow cytometry

Twenty-four hours after 17-DMAG treatment, SKOV-3 cells were harvested and washed with phosphate buffered saline (PBS) containing 0.5% bovine serum albumin (BSA). Upon blockade by 2% BSA in PBS, the cells were incubated with trastuzumab (10 μg/mL in PBS containing 2% BSA). FITC-conjugated donkey anti-human IgG was then added and allowed to incubate for 1 h at room temperature. After washing, the cells were analyzed using an LSR flow cytometer (Beckman Coulter, Fullerton, CA). The FITC signal intensity was analyzed using the Cell-Quest software (version 3.3, Becton-Dickinson, Franklin Lakes, NJ).

Western blot

At 8 hr and 24 hr after treated with 200nM 17-DMAG, SKOV3 cells were collected. Total protein was extracted using RIPA buffer (Pierce Biotechnology, Rockford, IL) plus 1mM EDTA, 1% Triton 100, 10% glycerol, and protease inhibitors. The concentration of total protein was determined using a microBCA protein assay kit (Pierce Biotechnology, Rockford, IL). After SDS-PAGE separation of 40 μg of total protein, it was transferred to a polyvinylidene fluoride membrane (Invitrogen, Carlsbad, CA) and incubated at room temperature with 5% non-fat milk blocking buffer. The blots were then incubated overnight at 4 °C with trastuzumab followed by incubation at room temperature for 1 h with horseradish peroxidase (HRP)-conjugated anti-human antibody and anti-rabbit antibody (GE

Healthcare, Piscataway, NJ). The bands were detected using an ECL western blotting detection system (GE Healthcare) with α-tubulin as loading control.

Tumor model and treatment protocol

All animal experiments were performed under a protocol approved by the Stanford University Administrative Panel on Laboratory Animal Care (A-PLAC). Subcutaneous SKOV-3 tumor models were established in 4 to 6-week-old male athymic nude mice. Typically, 5×10^6 cells suspended in 100 μl of serum-free DMEM medium were injected into the right front flank of the mice. The mice were subjected to microPET imaging studies when the tumor volume reached 200-400 mm^3 (3-4 weeks after inoculation). Animals in one group each received a total of 150 mg/kg of 17-DMAG dissolved in 10% DMSO and 10% Ethanol over 24 h in 3 doses of 50 mg/kg each. The control animals were each injected with equal amounts of DMSO/Ethanol without 17-DMAG. For therapy study, a dose of 50 mg/kg of 17-DMAG was given by tail vein injection for 3 consecutive days. Tumor growth was monitored by caliper measurement and tumor volume was calculated by the equation: Tumor volume (mm^3) = long diameter × (short diameter)^2/2.

MicroPET and image analysis

Detailed procedures for DOTA conjugation have been performed as previously described [34]. ^{64}Cu-DOTA-trastuzumab was purified by PD-10 column using PBS as the mobile phase. PET of tumor-bearing mice was performed on a microPET R4 rodent model scanner (Siemens Medical Solutions USA, Inc.). Twenty-four hours after 17-DMAG treatment, the mice were intravenously injected with ^{64}Cu-DOTA-trastuzumab (7-8 MBq/mouse) and static scans were acquired at 4 and 24 h post-injection (p.i.). For each microPET scan, 3-dimensional regions-of-interest (ROIs) were drawn over the tumor, liver, kidneys, and muscle on decay-corrected whole-body coronal images. The average radioactivity concentration within a tumor or an organ was obtained from the mean pixel values within the ROI volume, which were converted to counts per milliliter per minute by using a conversion factor. Assuming a tissue density of 1 g/ml, the counts per milliliter per minute were converted to counts per gram per minute and then divided by the injected dose (ID) to obtain an imaging ROI-derived %ID/g.

For FDG imaging, after a tail vein injection of 3.7 MBq of ^{18}F-FDG in 150 μL of PBS, a 7-min prone acquisition scan was performed approximately 60 min after injection. Mice were maintained under isoflurane anesthesia during the injection, accumulation, and scanning periods. PET images were analyzed and quantified as described above.

Biodistribution studies

After microPET imaging, mice bearing SKOV-3 tumor xenografts were sacrificed and dissected. Blood, tumor and major organs and tissues were collected and wet weighed. The radioactivity in each tissue was measured using a γ-counter (Packard Instrument) and the results were presented as % ID/g. For each mouse, the radioactivity of the tissue samples was calibrated against a known aliquot of the injectate and normalized to a body mass of 25 g. Values were expressed as mean ± SD for a group of 4 animals.

Immunofluorescence staining

Frozen SKOV-3 tumor sections (5 μm thick) were warmed to room temperature, fixed with ice-cold acetone for 10 min, and dried in the air for 30 min. The sections were rinsed in PBS for 2 min and blocked in 10% donkey serum for 1 h at room temperature. The sections were incubated with trastuzumab (10 μg/ml) for 1 h at room temperature and visualized with FITC-conjugated donkey anti-human secondary antibody (1:200, Jackson ImmunoResearch

Laboratories, West Grove, PA) under a microscope (Carl Zeiss Axiovert 200M, Carl Zeiss USA, Thornwood, NY). Images were acquired under the same conditions and displayed at the same scale.

Statistical analysis

Quantitative data were expressed as mean ± SD. Means were compared using one-way ANOVA and Student's t test. *P* values < 0.05 were considered statistically significant.

Results

17-DMAG inhibits SKOV-3 cell proliferation and induces HER-2 degradation

The effect of 17-DMAG on the proliferation of SKOV-3 cells was assessed by MTT colorimetric assay. We found that 17-DMAG inhibited cell proliferation in a dose-dependent manner (Fig. 1a). The IC_{50} value was about 34.58 nM at the 48 hour time point and 24.72 nM at the 72 hour time point.

17-DMAG has been reported to down-regulate HER-2 expression through the inhibition of Hsp90 function [35, 36]. Next we performed flow cytometry analysis using trastuzumab as the primary antibody to assess the effect of 17-DMAG on HER-2 expression level in SKOV-3 cells. As shown in Fig. 1b, 17-DMAG significantly decreased HER-2 expression in a dose dependent manner. The HER-2 level dropped by 15% after incubation with 100 nM of 17-DMAG for 24 h and by 65% with 500 nM of 17-DMAG. Western results (Fig. 1c) showed that as early as 8 hr after treated with 17-DMAG, HER-2 protein level began to decrease, indicating that it is possible to detect the early response of SKOV-3 cells to 17-DMAG treatment by monitoring HER-2 degradation.

Imaging HER-2 expression with microPET

^{64}Cu-DOTA-trastuzumab was determined to have around 20 DOTA residues per trastuzumab [37]. Flow cytometry analysis with DOTA-trastuzumab showed that after DOTA conjugation, the antibody still keeps relative high binding affinity with HER-2 (Fig. 2a). The specific activity of ^{64}Cu-DOTA-trastuzumab was 1.36 ± 0.15 GBq/mg mAb and the radiolabeling yield was around 85%. PET scans were performed at different time points after i.v. injection of 3.7 MBq of ^{64}Cu-DOTA-trastuzumab to SKOV3 tumor bearing nude mice. As seen in Fig. 2b, the SKOV-3 tumor uptake of ^{64}Cu-DOTA-trastuzumab was increased with time and almost reached a plateau at about 24-hour p.i. The tumor uptake was 2.39 ± 0.76, 6.13 ± 2.30, 19.85 ± 0.83 and 25.69 ± 3.10 % ID/g at 1-, 4-, 24- and 48-hour p.i., respectively. ^{64}Cu-DOTA-trastuzumab exhibited high uptake in the heart (due to the blood pool activity) and liver at early time points, whereas the tracer uptake in all the other organs was at the background level (Fig. 2b). As shown in Fig. 2c, the tracer uptake in both the heart and the liver dropped steadily over time. For the heart, the uptake was 29.68 ± 4.05, 22.15 ± 6.11, 12.34 ± 5.54 and 9.72 ± 6.58 %ID/g at 1-, 4-, 24- and 48-hour p.i., respectively. For the liver, the uptake was 23.25 ± 1.92, 16.91± 1.33, 11.81 ± 1.64 and 10.45 ± 1.38 %ID/g at at 1-, 4-, 24- and 48-hour p.i., respectively.

microPET imaging of HER-2 degradation

In order to image the HER-2 changes after 17-DMAG treatment, PET scans were performed in SKOV-3 tumor bearing animals 24 hr after single dose of 17-DMAG treatment. The decay-corrected whole-body coronal images containing the tumors are shown in Fig. 3a. After being treated with 150 mg/kg of 17-DMAG for 24 h, the SKOV-3 tumor uptake of ^{64}Cu-DOTA-trastuzumab was much lower in both early and late time points as compared with the untreated group. Quantitative data based on ROI analysis are shown in Fig. 3b. In untreated mice, the SKOV-3 tumor uptake of ^{64}Cu-DOTA-trastuzumab was 10.96 ± 0.93 %

ID/g and 33.90 ± 7.82 % ID/g at 4 and 24 hr p.i., respectively. The uptake in 17-DMAG treated tumors was significantly lower, with 4.75 ± 2.41 %ID/g and 11.74 ± 4.23 %ID/g at 4 and 24 hr p.i. respectively ($P < 0.05$ at both time points). There were no significant differences in ^{64}Cu-DOTA-trastuzumab uptake in other major organs between the 17-DMAG treated and untreated animals.

Biodistribution studies

After microPET imaging at 24 h p.i., the animals were sacrificed for biodistribution studies and the results are shown in Fig. 4a. The untreated SKOV-3 tumors had a high tracer uptake of 33.43 ± 8.93 %ID/g, consistent with the non-invasive microPET imaging results. After 17-DMAG treatment, the uptake decreased significantly to 10.08 ± 0.71 %ID/g ($P < 0.01$). Blood activity concentration was 15.38 ± 6.09 and 15.61 ± 4.71 %ID/g in 17-DMAG treated and control group, indicating the relative long circulation half-life of the antibody. The liver also had prominent radioactivity accumulation, with an uptake of 8.17 ± 1.79 and 7.71 ± 1.40 %ID/g at 24 hr p.i., due to both the hepatic clearance of antibody-based tracer and possible trans-chelation. Spleen also had similar uptake with liver.

Immunofluorescence staining

To further confirm that 17-DMAG induces HER-2 degradation in vivo, we performed immunofluorescence staining using trastuzumab as the primary antibody and FITC conjugated donkey anti-human IgG as the secondary antibody. Images were taken under the same condition and displayed at the same scale to make sure that the relative brightness observed in the images reflected the difference in HER-2 expression level. In the untreated SKOV-3 tumor, HER-2 expression was very high as indicated by the strong pseudo-colored green signal in the tissue. After being treated with 17-DMAG, HER-2 expression was apparently lower with a much weaker fluorescence signal (Fig. 4b). Both the biodistribution and immunofluorescence staining studies confirmed that the decrease in tumor HER-2 expression level upon 17-DMAG treatment can be non-invasively monitored by ^{64}Cu-DOTA-trastuzumab PET.

17-DMAG inhibits SKOV-3 tumor growth

The effects of 17-DMAG on both the tumor volume and body weight are shown in Fig. 5a and 5b, respectively. 17-DMAG is relatively non-toxic as no significant difference in mouse body weight between the control and treated animals. After treatment with 17-DMAG, the tumor growth was delayed and the tumor size was significantly smaller than the control group by day 12 ($P < 0.01$). The tumors in the control animals continued to grow exponentially with an apparent doubling time of 5.1 d and increased in size by a factor of 6.1 by day 16. In comparison, the 17-DMAG treated animals were only increased in size by a factor of 3.3 by day 16 (Fig. 5a).

Imaging of HER-2 changes during the therapeutic process

At day 7 after the first dose of 17-DMAG, i.e. day 3 after the last dose, the animals were scanned with ^{18}F-FDG and ^{64}Cu-DOTA-trastuzumab in tandem (Fig. 6). All tumors showed relatively high uptake of FDG. However, there is no significant difference between the therapeutic group (4.85 ± 0.73 %ID/g) and the control group (4.95 ± 0.82 % ID/g). In contrast, control tumors showed much higher accumulation of ^{64}Cu-DOTA-trastuzumab (25.68 ± 5.33 % ID/g) at 24 hr p.i. than that of 17-DMAG treated group (12.86 ± 2.41 % ID/g). The tumors showed low ^{64}Cu-DOTA-IgG uptake (5.34 ± 1.24 %ID/g), further confirming the specificity of ^{64}Cu-DOTA-trastuzumab and low non-specific targeting of antibodies in SKOV-3 tumor models.

Discussion

It has been reported that HSP90 inhibitor, 17-DMAG is a more effective cytotoxic agent than 17-AAG in gynecologic cancer cells by affecting multiple downstream pathways including EGFR/HER2 and Akt/PTEN [38]. The anti-tumor efficacy of 17-DMAG has also been confirmed in human breast and melanoma tumor models [39]. In this study, we treated SKOV-3 human ovarian cancer model with 17-DMAG and both *in vitro* and *in vivo* data supported that 17-DMAG is a potent anti-cancer agent. During the therapeutic process, we performed microPET imaging with ^{64}Cu-labeled anti-HER-2 mAb trastuzumab for the non-invasive monitoring of HER-2 expression and degradation.

Accurate evaluation of the HER-2 status in tumors by non-invasive molecular imaging will be critical for HER-2 related therapies. HER-2 itself is an intensively investigated therapeutic target and trastuzumab is the first monoclonal antibody approved by the Food and Drug Administration (FDA). Guidelines of the American Society of Clinical Oncology (ASCO) recommend evaluation of HER-2 expression on every primary breast cancer either at the time of diagnosis or at the time of recurrence [40]. Moreover, as a key component in promoting cell proliferation, HER-2 is closely related to other therapeutics such as HSP90 inhibitors as performed in this study or histone deacetylase (HDAC) inhibitors [41, 42]. Through monitoring the status of HER-2, the early response to certain drugs or potential drug candidates can be assessed. In this study, a series of imaging studies were carried out to evaluate HER-2 expression level. First, ^{64}Cu-DOTA-trastuzumab accumulation was clearly visualized on untreated SKOV-3 tumors, reaching a plateau from 24 hr to 48 hr p.i. Second, the tumor accumulation of ^{64}Cu-DOTA-trastuzumab was significantly lower in 17-DMAG treated animals (3 × 50 mg/kg 17-DMAg administered within 24 hr) than in untreated animals (11.74 ± 4.23 % ID/g vs. 33.90 ± 7.82 % ID/g 24 hr p.i.), which corroborates with the direct tissue sampling biodistribution studies of the same animals after the microPET scans. The HER-2 degradation was further confirmed by *ex vivo* immunofluorescent staining. Finally, we treated the animals with 3 × 50 mg/kg 17-DMAG for three consecutive days and measured the tumor size to observe the therapeutic efficacy of 17-DMAG. ^{18}F-FDG PET was performed at day 4 since the start of the treatment and ^{64}Cu-DOTA-trastuzumab PET at day 5. Again, tumor accumulation of ^{64}Cu-DOTA-trastuzumab was significantly lower in 17-DMAG treated group than that in control group as reflected on the quantitative microPET images. In contrast, FDG PET was unable to differentiate the treated from untreated. Smith-Jones *et al.* previously imaged HER-2 level in 17-AAG treated BT-474 human breast cancer model and found that the decrease of HER-2 level lasted for at least 7 days [43]. The results from our experiment are consistent with their findings.

Despite the high affinity for HER-2 antigen and high accumulation in HER-2 positive tumors, ^{64}Cu-DOTA-trastuzumab has relatively slow clearance that makes it unsuitable for multiple scans within short time intervals. For such purposes, suitably labeled small molecules, peptides, antibody fragments, or affibodies might have advantage over intact monoclonal antibodies [44, 45]. Overall, antibodies are still the best established class of binding molecules for tumor diagnosis and therapy [23, 46]. Comparing with antibody fragments and affibodies, whole antibodies are superior in both affinity and specificity to the targets. In addition, much lower kidney accumulation may be an add-on for ovarian cancer localization and evaluation. Finally, ^{64}Cu-DOTA-trastuzumab PET imaging will be more appropriate to the situation in which HSP90 inhibitors were combined with trastuzumab for synergistic tumor control. Since HER-2 is one of the most sensitive client proteins of HSP90 [6], it is not surprising to see synergistic effect when combining HSP90 inhibition and anti-HER-2 therapy. Indeed, it has been reported that the combination of trastuzumab and 17-AAG induced enhanced HER-2 degradation and cytotoxicity in HER-2 overexpressing breast cancer cells [47]. More importantly, the synergistic growth arrest and cell death was

not observed in cancer cells with low HER-2 expression. This synergistic effect was further substantiated by a phase I/II trial which showed multiple partial responses in HER-2 positive metastatic breast cancer patients using 17-AAG plus trastuzumab [48]. It is worth mentioning that the same dose and schedule of 17-AAG was used in this trial as the other failed clinical trials described earlier [19]. With ^{64}Cu-DOTA-trastuzumab PET imaging, more comprehensive information can be retrieved non-invasively including HER-2 expression status, antibody delivery and distribution and early response to the combined treatment.

Conclusion

We describe here the use of quantitative HER-2 PET imaging with ^{64}Cu-DOTA-trastuzumab for monitoring the early therapeutic response upon 17-DMAG treatment in aSKOV-3 human ovarian cancer model. The quantification of HER-2 degradation during 17-DMAG treatment using PET imaging is consistent with the *in vitro* and *ex vivo* measurements. This approach may be clinically translated to monitor the therapeutic response in HER-2-positive cancer patients under 17-DMAG treatment and to select patients for 17-DMAG and trastuzumab combination therapy.

Acknowledgments

This work was supported by the National Cancer Institute (NCI) P50 CA114747 and a DOD Prostate Postdoctoral Fellowship from Department of Defense (to G. Niu).

References

1. Jakob U, Lilie H, Meyer I, Buchner J. Transient interaction of Hsp90 with early unfolding intermediates of citrate synthase. Implications for heat shock in vivo. J Biol Chem. 1995; 270:7288–94. [PubMed: 7706269]
2. Blagosklonny MV, Toretsky J, Bohen S, Neckers L. Mutant conformation of p53 translated in vitro or in vivo requires functional HSP90. Proc Natl Acad Sci U S A. 1996; 93:8379–83. [PubMed: 8710879]
3. Clarke PA, Hostein I, Banerji U, Stefano FD, Maloney A, Walton M, et al. Gene expression profiling of human colon cancer cells following inhibition of signal transduction by 17-allylamino-17-demethoxygeldanamycin, an inhibitor of the hsp90 molecular chaperone. Oncogene. 2000; 19:4125–33. [PubMed: 10962573]
4. Burrows F, Zhang H, Kamal A. Hsp90 activation and cell cycle regulation. Cell Cycle. 2004; 3:1530–6. [PubMed: 15539946]
5. Solit DB, Zheng FF, Drobnjak M, Münster PN, Higgins B, Verbel D, et al. 17-Allylamino-17-demethoxygeldanamycin induces the degradation of androgen receptor and HER-2/neu and inhibits the growth of prostate cancer xenografts. Clinical cancer research. 2002; 8:986–93. [PubMed: 12006510]
6. Basso AD, Solit DB, Munster PN, Rosen N. Ansamycin antibiotics inhibit Akt activation and cyclin D expression in breast cancer cells that overexpress HER2. Oncogene. 2002; 21:1159–66. [PubMed: 11850835]
7. Pratt WB, Toft DO. Regulation of signaling protein function and trafficking by the hsp90/hsp70-based chaperone machinery. Exp Biol Med (Maywood). 2003; 228:111–33. [PubMed: 12563018]
8. Schechter AL, Hung MC, Vaidyanathan L, Weinberg RA, Yang-Feng TL, Francke U, et al. The neu gene: an erbB-homologous gene distinct from and unlinked to the gene encoding the EGF receptor. Science. 1985; 229:976–78. [PubMed: 2992090]
9. Tan M, Yao J, Yu D. Overexpression of the c-erbB-2 gene enhanced intrinsic metastasis potential in human breast cancer cells without increasing their transformation abilities. Cancer Res. 1997; 57:1199–205. [PubMed: 9067293]

10. Bacus SS, Ruby SG, Weinberg DS, Chin D, Ortiz R, Bacus JW. HER-2/neu oncogene expression and proliferation in breast cancers. Am J Pathol. 1990; 137:103–11. [PubMed: 1973597]
11. Wiercioch R, Balcerczak E, Byszewska E, Mirowski M. Uptake of radiolabelled herceptin by experimental mammary adenocarcinoma. Nucl Med Rev Cent East Eur. 2003; 6:99–103. [PubMed: 14737722]
12. Traish AM, Wotiz HH. Prostatic epidermal growth factor receptors and their regulation by androgens. Endocrinology. 1987; 121:1461–7. [PubMed: 3498628]
13. Fischer U, Kopka L, Brinck U, Korabiowska M, Schauer A, Grabbe E. Prognostic value of contrast-enhanced MR mammography in patients with breast cancer. Eur Radiol. 1997; 7:1002–5. [PubMed: 9265662]
14. Citri A, Alroy I, Lavi S, Rubin C, Xu W, Grammatikakis N, et al. Drug-induced ubiquitylation and degradation of ErbB receptor tyrosine kinases: implications for cancer therapy. Embo J. 2002; 21:2407–17. [PubMed: 12006493]
15. Murakami Y, Mizuno S, Uehara Y. Accelerated degradation of 160 kDa epidermal growth factor (EGF) receptor precursor by the tyrosine kinase inhibitor herbimycin A in the endoplasmic reticulum of A431 human epidermoid carcinoma cells. Biochem J. 1994; 301(Pt 1):63–8. [PubMed: 8037692]
16. Kelland LR, Sharp SY, Rogers PM, Myers TG, Workman P. DT-Diaphorase expression and tumor cell sensitivity to 17-allylamino, 17-demethoxygeldanamycin, an inhibitor of heat shock protein 90. J Natl Cancer Inst. 1999; 91:1940–9. [PubMed: 10564678]
17. Silcox CE, Smith RC, King R, McDannold N, Bromley P, Walsh K, et al. MRI-guided ultrasonic heating allows spatial control of exogenous luciferase in canine prostate. Ultrasound Med Biol. 2005; 31:965–70. [PubMed: 15972202]
18. Sausville EA, Tomaszewski JE, Ivy P. Clinical development of 17-allylamino, 17-demethoxygeldanamycin. Curr Cancer Drug Targets. 2003; 3:377–83. [PubMed: 14529389]
19. Solit DB, Osman I, Polsky D, Panageas KS, Daud A, Goydos JS, et al. Phase II trial of 17-allylamino-17-demethoxygeldanamycin in patients with metastatic melanoma. Clin Cancer Res. 2008; 14:8302–7. [PubMed: 19088048]
20. Ronnen EA, Kondagunta GV, Ishill N, Sweeney SM, Deluca JK, Schwartz L, et al. A phase II trial of 17-(Allylamino)-17-demethoxygeldanamycin in patients with papillary and clear cell renal cell carcinoma. Invest New Drugs. 2006; 24:543–6. [PubMed: 16832603]
21. Barzilay E, Ben-Califa N, Supino-Rosin L, Kashman Y, Hirschberg K, Elazar Z, et al. Geldanamycin-associated inhibition of intracellular trafficking is attributed to a co-purified activity. J Biol Chem. 2004; 279:6847–52. [PubMed: 14660597]
22. Lang SA, Klein D, Moser C, Gaumann A, Glockzin G, Dahlke MH, et al. Inhibition of heat shock protein 90 impairs epidermal growth factor-mediated signaling in gastric cancer cells and reduces tumor growth and vascularization in vivo. Mol Cancer Ther. 2007; 6:1123–32. [PubMed: 17363505]
23. Smith MA, Morton CL, Phelps DA, Kolb EA, Lock R, Carol H, et al. Stage 1 testing and pharmacodynamic evaluation of the HSP90 inhibitor alvespimycin (17-DMAG, KOS-1022) by the pediatric preclinical testing program. Pediatr Blood Cancer. 2008; 51:34–41. [PubMed: 18260120]
24. Niu G, Chen X. Has molecular and cellular imaging enhanced drug discovery and drug development? Drugs R D. 2008; 9:351–68. [PubMed: 18989988]
25. McManus DT, Patterson AH, Maxwell P, Humphreys MW, Anderson NH. Fluorescence in situ hybridisation detection of erbB2 amplification in breast cancer fine needle aspirates. Mol Pathol. 1999; 52:75–7. [PubMed: 10474685]
26. Stomper PC, Budnick RM, Stewart CC. Use of specimen mammography-guided FNA (fine-needle aspirates) for flow cytometric multiple marker analysis and immunophenotyping in breast cancer. Cytometry. 2000; 42:165–73. [PubMed: 10861689]
27. Tokunaga E, Oki E, Nishida K, Koga T, Egashira A, Morita M, et al. Trastuzumab and breast cancer: developments and current status. Int J Clin Oncol. 2006; 11:199–208. [PubMed: 16850126]
28. Thrall JH. Personalized Medicine. Radiology. 2004; 231:613–16. 10.1148/radiol.2313040323 10.1148/radiol.2313040323. [PubMed: 15163802]

29. Shepard HM, Lewis GD, Sarup JC, Fendly BM, Maneval D, Mordenti J, et al. Monoclonal antibody therapy of human cancer: taking the HER2 protooncogene to the clinic. J Clin Immunol. 1991; 11:117–27. [PubMed: 1679763]
30. Carter P, Presta L, Gorman CM, Ridgway JB, Henner D, Wong WL, et al. Humanization of an anti-p185HER2 antibody for human cancer therapy. Proc Natl Acad Sci U S A. 1992; 89:4285–9. [PubMed: 1350088]
31. Bulte JWM, Kraitchman DL. Iron oxide MR contrast agents for molecular and cellular imaging. NMR in Biomedicine. 2004; 17:484–99. [PubMed: 15526347]
32. Lee JH, Huh YM, Jun YW, Seo JW, Jang JT, Song HT, et al. Artificially engineered magnetic nanoparticles for ultra-sensitive molecular imaging. Nat Med. 2007; 13:95–9. [PubMed: 17187073]
33. Lub-de Hooge MN, Kosterink JG, Perik PJ, Nijnuis H, Tran L, Bart J, et al. Preclinical characterisation of ^{111}In-DTPA-trastuzumab. Br J Pharmacol. 2004; 143:99–106. [PubMed: 15289297]
34. Niu G, Cai W, Chen K, Chen X. Non-invasive PET imaging of EGFR degradation induced by a heat shock protein 90 inhibitor. Mol Imaging Biol. 2008; 10:99–106. [PubMed: 18157579]
35. Konecny GE, Pegram MD, Venkatesan N, Finn R, Yang G, Rahmeh M, et al. Activity of the dual kinase inhibitor lapatinib (GW572016) against HER-2-overexpressing and trastuzumab-treated breast cancer cells. Cancer Res. 2006; 66:1630–9. [PubMed: 16452222]
36. Lang W, Caldwell GW, Li J, Leo GC, Jones WJ, Masucci JA. Biotransformation of geldanamycin and 17-allylamino-17-demethoxygeldanamycin by human liver microsomes: reductive versus oxidative metabolism and implications. Drug Metab Dispos. 2007; 35:21–9. [PubMed: 17012542]
37. Cai W, Wu Y, Chen K, Cao Q, Tice DA, Chen X. In vitro and in vivo characterization of 64Cu-labeled Abegrin, a humanized monoclonal antibody against integrin alpha v beta 3. Cancer Res. 2006; 66:9673–81. [PubMed: 17018625]
38. Gossett DR, Bradley MS, Jin X, Lin J. 17-Allyamino-17-demethoxygeldanamycin and 17-NN-dimethyl ethylene diamine-geldanamycin have cytotoxic activity against multiple gynecologic cancer cell types. Gynecol Oncol. 2005; 96:381–8. [PubMed: 15661225]
39. Hollingshead M, Alley M, Burger AM, Borgel S, Pacula-Cox C, Fiebig HH, et al. In vivo antitumor efficacy of 17-DMAG (17-dimethylaminoethylamino-17-demethoxygeldanamycin hydrochloride), a water-soluble geldanamycin derivative. Cancer Chemother Pharmacol. 2005; 56:115–25. [PubMed: 15791458]
40. Bast RC, Ravdin P, Hayes DF, Bates S, Fritsche H, Jessup JM, et al. 2000 update of recommendations for the use of tumor markers in breast and colorectal cancer: clinical practice guidelines of the American Society of Clinical Oncology. Journal of clinical oncology. 2001; 19:1865–78. [PubMed: 11251019]
41. Strahl BD, Allis CD. The language of covalent histone modifications. Nature. 2000; 403:41–45. [PubMed: 10638745]
42. Turner BM. Cellular memory and the histone code. Cell. 2002; 111:285–91. [PubMed: 12419240]
43. Smith-Jones PM, Solit DB, Akhurst T, Afroze F, Rosen N, Larson SM. Imaging the pharmacodynamics of HER2 degradation in response to Hsp90 inhibitors. Nat Biotechnol. 2004; 22:701–6. [PubMed: 15133471]
44. Smith-Jones PM, Solit D, Afroze F, Rosen N, Larson SM. Early tumor response to Hsp90 therapy using HER2 PET: comparison with ^{18}F-FDG PET. J Nucl Med. 2006; 47:793–6. [PubMed: 16644749]
45. Orlova A, Tolmachev V, Pehrson R, Lindborg M, Tran T, Sandstrom M, et al. Synthetic affibody molecules: a novel class of affinity ligands for molecular imaging of HER2-expressing malignant tumors. Cancer Res. 2007; 67:2178–86. [PubMed: 17332348]
46. Bernier J. Drug Insight: cetuximab in the treatment of recurrent and metastatic squamous cell carcinoma of the head and neck. Nat Clin Pract Oncol. 2008
47. Raja SM, Clubb RJ, Bhattacharyya M, Dimri M, Cheng H, Pan W, et al. A combination of Trastuzumab and 17-AAG induces enhanced ubiquitinylation and lysosomal pathway-dependent ErbB2 degradation and cytotoxicity in ErbB2-overexpressing breast cancer cells. Cancer Biol Ther. 2008; 7:1630–40. [PubMed: 18769124]

48. Modi S, Stopeck AT, Gordon MS, Mendelson D, Solit DB, Bagatell R, et al. Combination of trastuzumab and tanespimycin (17-AAG, KOS-953) is safe and active in trastuzumab-refractory HER-2 overexpressing breast cancer: a phase I dose-escalation study. J Clin Oncol. 2007; 25:5410–7. [PubMed: 18048823]

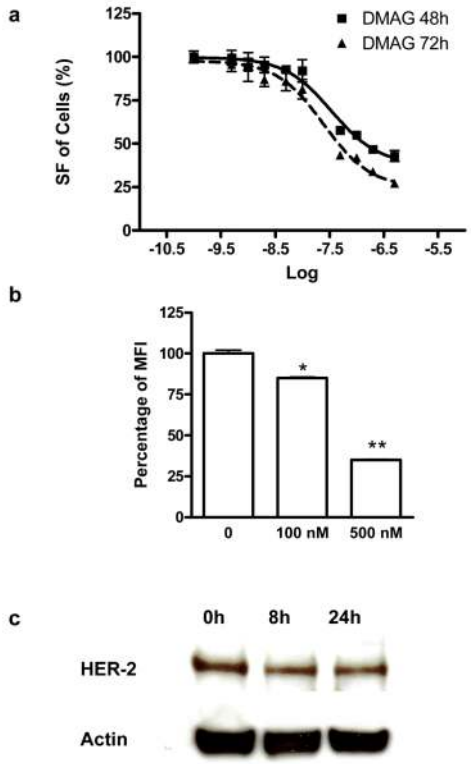

Fig. 1.

a The cytotoxic effect of 17-DMAG on SKOV-3 human ovarian cancer cells. SKOV-3 cells were treated with serial concentrations of 17-DMAG. At 48 and 72 hr after treatment, the cell proliferation was determined by MTT assay. **b** Flow cytometric analysis of HER-2 expression on SKOV-3 cells after being treated with different concentrations of 17-DMAG. Trastuzumab was used as the primary antibody and FITC-conjugated donkey anti-human IgG as the secondary antibody. The mean value of FITC signal intensity (MFI) of the three measurements were also shown (mean ± SD). **c** Western blot of HER-2 in SKOV-3 cells treated or untreated with 200nM of 17-DMAG. Trastuzumab was used as the primary mAb. *, $P < 0.05$; **, $P < 0.01$.

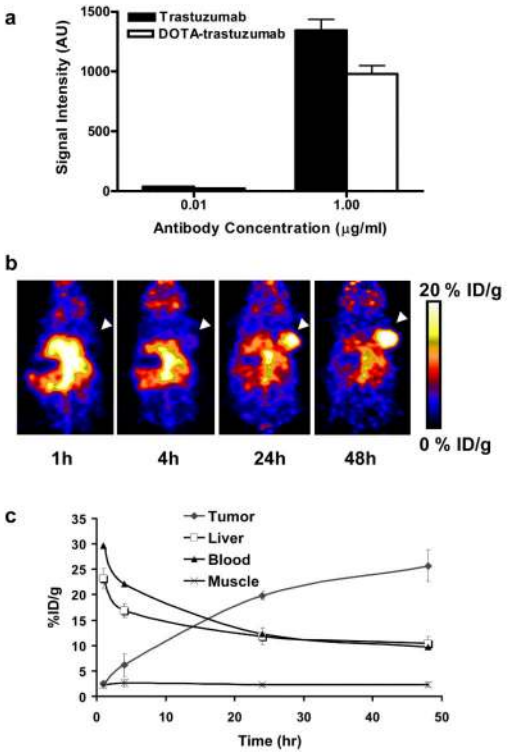

Fig. 2.

a Flow cytometric analysis of HER-2 expression on SKOV-3 cells with DOTA conjugated trastuzumab as the primary antibody. The mean value of FITC signal intensity (MFI) of the three measurements were also shown (mean ± SD). **b** MicroPET images of SKOV-3 tumor-bearing nude mice at different time points after intravenous injection of ^{64}Cu-DOTA-trastuzumab (n = 4/group). Decay-corrected whole-body coronal images were shown and the tumors were indicated by white arrows. **c** SKOV-3 tumor and major organ uptake of ^{64}Cu-DOTA-trastuzumab as quantified from microPET scans (n=4/group).

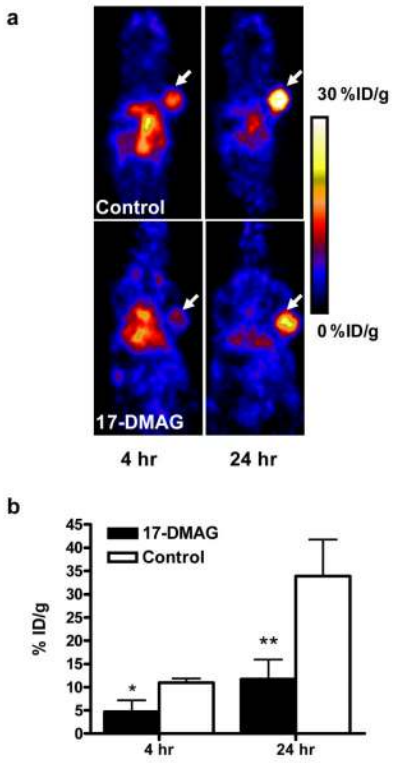

Fig. 3.

a MicroPET images of SKOV-3 tumor-bearing nude mice treated with or without 17-DMAG at 4 and 24 hr after intravenous injection of ^{64}Cu-DOTA-trastuzumab (n = 4/group). Decay-corrected whole-body coronal images were shown and the tumors were indicated by white arrows. **b** SKOV-3 tumor uptake of ^{64}Cu-DOTA-trastuzumab as quantified from microPET scans (n=4/group).

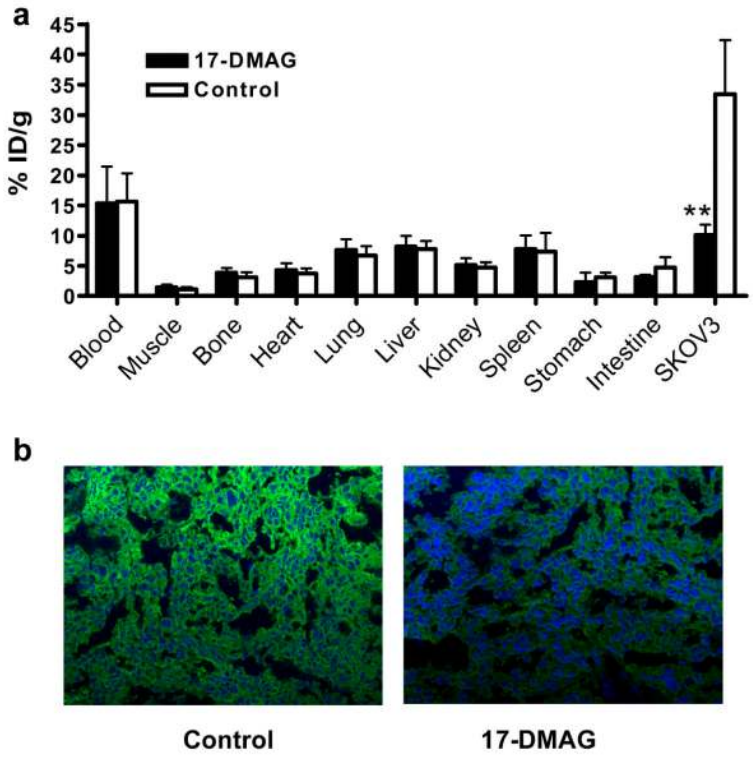

Fig. 4.

a Biodistribution of ^{64}Cu-DOTA-trastuzumab (with or without 17-DMAG treatment) in SKOV-3 tumor-bearing mice at 24 h post-injection (n = 4/group). **b** Immunofluorescence staining of HER-2 in 17-DMAG treated and untreated SKOV-3 tumor tissues. Images were obtained under the same conditions and displayed at the same magnification and scale (200×). *, $P < 0.05$; **, $P < 0.01$.

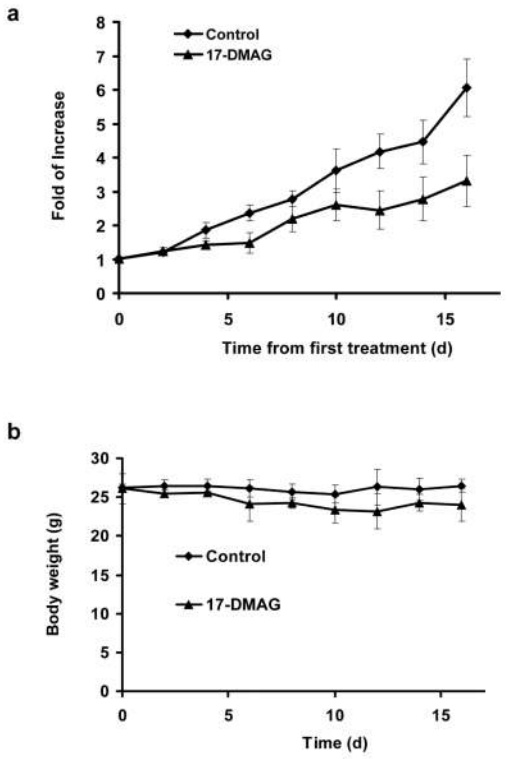

Fig. 5.

a Comparison of SKOV-3 tumor growth in nude mice treated with 17-DMAG vs. control animals. **b** Comparison of body mass of nude mice treated with 17-DMAG vs. control animals. Animals were treated with 17-DMAG (50 mg/kg/day) for 3 consecutive days.

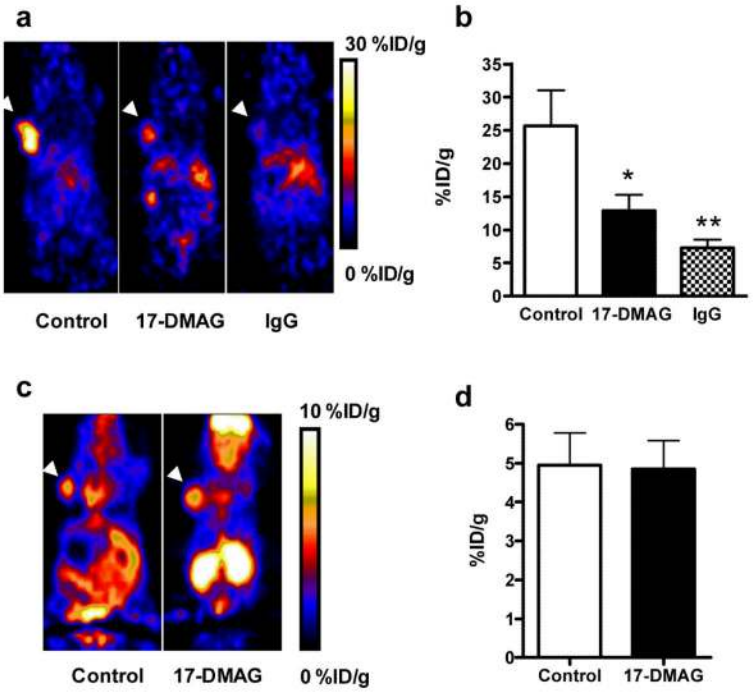

Fig. 6.

a MicroPET images of SKOV-3 tumor-bearing nude mice with ^{64}Cu-DOTA-trastuzumab at day 5 after being treated with 17-DMAG (n = 4 to 7/group). Decay-corrected whole-body coronal images were shown and the tumors were indicated by white arrow heads. **b** SKOV-3 tumor uptake of ^{64}Cu-DOTA-trastuzumab as quantified from microPET scans (n=4 to 7/group). **c** MicroPET images of SKOV-3 tumor-bearing nude mice with ^{18}F-FDG at day 5 after treatment with 17-DMAG (n = 4 to 7/group). Decay-corrected whole-body coronal images were shown and the tumors were indicated by white arrow heads. **d** SKOV-3 tumor uptake of ^{18}F-FDG as quantified from microPET scans (n= 4 to 7/group). *, $P < 0.05$; **, $P < 0.01$.